In: Visual Cortex: New Research
Editors: T. A. Portocello and R. B. Velloti

ISBN 978-1-60456-530-0

Chapter 4

LARGE- AND SMALL-SCALE FUNCTIONAL ORGANIZATION OF VISUAL FIELD REPRESENTATION IN THE HUMAN VISUAL CORTEX

Hiroki Yamamoto[1*], Hiroshi Ban[1, 2], Masaki Fukunaga[3], Chuzo Tanaka[4], Masahiro Umeda[3] and Yoshimichi Ejima[5]

[1]Department of Human Coexistence, Graduate School of Human and Environmental Studies, Kyoto University, Kyoto, Japan
[2]KOKORO Research Center, Kyoto University, Kyoto, Japan
[3]Department of Medical Informatics,
Meiji University of Oriental Medicine, Kyoto, Japan
[4]Department of Neurosurgery, Meiji University of Oriental Medicine, Kyoto, Japan
[5]Kyoto Institute of Technology, Kyoto, Japan

Abstract

A fundamental characteristic of the human visual cortex is its retinotopic organization. Taking advantage of the systematic association between cortical position and visual field position, many important aspects of visual processing have been revealed by functional brain imaging. We have investigated, visualized, and characterized retinotopic organization using fMRI, in conjunction with several novel methods of analysis. In this chapter, we describe the methodology used and present findings on the basic functional organization of the visual cortex from two interlocking large- and small-scale perspectives. By larger-scale analyses of retinotopic organization, we have been able to delineate hierarchically organized visual areas (V1, V2, V3, V3A, V3B, V4v, V8, LOc, and MT+) for ten hemispheres and investigated their individual variability in size and location using a probabilistic approach, in which probability maps of the visual areas were created. With smaller-scale analyses of retinotopy, we obtained two basic factors of visual field representation within each area (cortical magnification factor and average receptive field size), and with these factors estimated the cortical point spread of fMRI activity. We found that point spread is nearly constant across eccentricities and

* Correspondence to: Dr. Hiroki Yamamoto. Department of Human Coexistence, Graduate School of Human and Environmental Studies, Kyoto University, Yoshida Nihonmatsu-cho, Sakyo-ku, Kyoto 606-8501, Japan, E-mail: yamamoto@cv.jinkan.kyoto-u.ac.jp, Tel: +81-75-753-2978; Fax: +81-75-753-6574

increases as one ascends the visual cortical hierarchy. Knowledge of retinotopic organization is important not only in itself; it also provides essential information for analysis and interpretation of functional activity in visual cortex. As representative examples, we present our recent findings on visual functions involving contextual effects. The present findings on the large- and small-scale functional organization of the human visual cortex shed new light on the relationship between functional segregation and cortical processing hierarchy in the visual system.

Keywords: retinotopy, probabilistic atlas, magnification factor, point spread, contextual effects, fMRI.

1. Introduction

Functional brain imaging, including positron emission tomography (PET) and functional magnetic resonance imaging (fMRI), provides strong clues to understanding the functional organization of the human visual cortex. Although this understanding is far from complete, recent advances in imaging technology have enabled investigation of brain functional activity at mm-order resolution across the cortical surface [1] and thereby yielded detailed maps of the functions of its many zones [2, 3].

Over the last decade or two, brain mapping studies of human visual cortex have revealed two major principles of its functional organization. The first is organization with respect to visual categories. Following the discovery of the color center, exhibiting high selectivity for color [4], multiple zones, seemingly specialized for representing different visual attributes such as color, shape, face, and motion, have been found within occipito-temporal cortex [3, 5-7]. The demonstration of such functional specialization has been one major criterion for defining high-level visual areas dedicated to the processing of specific visual categories.

The second principle is organization with respect to the retinal and visual field positions being represented. Visual neurons respond only to stimuli located in a finite region of the visual field known as the classical receptive field (RF). In many parts of the visual cortex, the RF centers of neurons all point to the same location in visual space with some scatter if they reside at the same cortical location, and RF center position gradually shifts over the cortex [8, 9]. This systematic association between cortical position and visual field position is termed retinotopy. Like functional specialization, evidence for a single complete retinotopic representation of the entire visual field has been an important criterion for defining a visual area [10, 11].

The present paper focuses on the second organizational principle of retinotopy in the human visual cortex. We describe our findings on retinotopic organization along with two interlocking large- and small-scale perspectives, placing special emphasis on experimental techniques and analysis. By larger- scale analyses of retinotopic organization, we have delineated multiple visual areas and investigated their individual variability in size and location using a probabilistic approach. With smaller-scale analyses of retinotopy, we have obtained two basic factors of visual field representation (cortical magnification factor and average receptive field size), and from these factors estimated the cortical point spread of fMRI activity. Knowledge of retinotopic organization is important not only in itself; it also provides essential information for analysis and interpretation of functional activity in visual cortex. As representative examples, we present our recent findings on visual functions

involving visual contextual effects. Unless mentioned otherwise, the analyses described in this chapter were performed and visualized using in-house software [12, 13] written in VTK (Kitware, Clifton Park, NY) and MATLAB (Mathworks, Natick, MA).

2. Retinotopic Organization of Human Visual Cortex

Polar Coordinate Representation of the Visual Field

We have measured retinotopic organization with fMRI [14-18] using a phase-encoding technique in which receptive field centers are temporally coded using polar coordinates [19]. An overview of the method and results for the region that surrounds the right calcarine sulcus are presented in Figure 1. Eccentricity and polar angle were measured by performance of fMRI while the subject viewed a checkered annulus that expanded from the fovea to 16° peripherally (Figure 1A) or a wedge-shaped checkered pattern rotated around the fixation point (Figure 1B), respectively. Each stimulus was presented repeatedly with a 60s period, evoking a periodic response at a given point on retinotopic cortex, whose corresponding position in the visual field was encoded in the phase of its 60s periodic component and thus could be estimated using Fourier analysis (Figure 1C, D). Comparison of Figure 1C and D

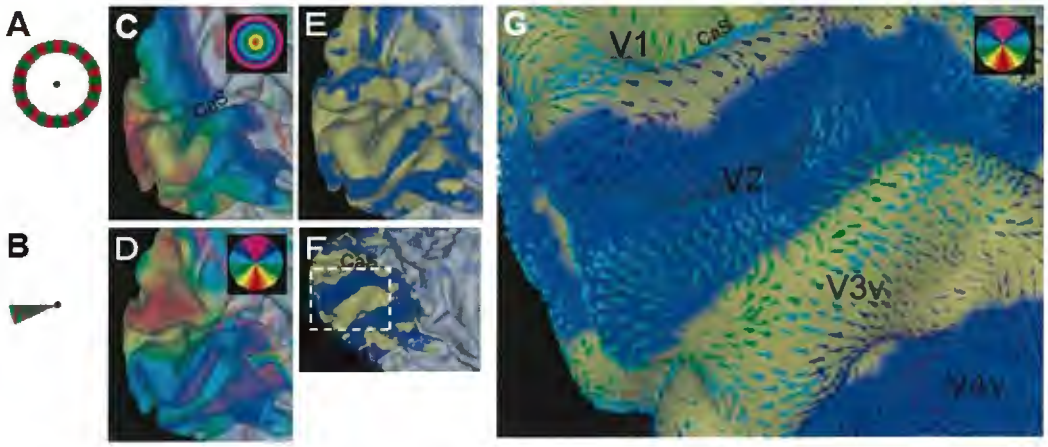

Figure 1. Phase-encoding method for measurements of retinotopy. (A) The thin (2 °) annulus expanded from the fovea to 16° periphery repeatedly with a 60s period in the eccentricity mapping experiment. (B) The wedge (24°) rotated around the fixation point repeatedly with a 60s period. (C) The eccentricity map around the calcarine sulcus. The color overlay on the cortex indicates the preferred stimulus eccentricity at each cortical point, in accordance with the color code in the upper right. (D) The polar angle map, presented in the same format as C. (E) Field sign map. The yellow region indicates the mirror image representation, while the blue indicates the non-mirror image. (F) Field sign map for the region ventral to the calcarine sulcus. (G) Zoom-in of F. Each triangular glyph represents the direction of the gradient at the point in the polar angle map, the colors of which code polar angle as in D. Note that the directions of the gradients reverse at the border of the mirror/non-mirror representation.

shows that the eccentricity and polar angle of the visual field are represented systematically in orthogonal maps around the calcarine sulcus. Figure 1C shows that the posterior part

represents central vision and the more anterior part peripheral vision. Figure 1D shows that the regions dorsal and ventral to the calcarine sulcus, respectively, represent the lower and upper contralateral quadrants of the visual field. Notably, the quarter-field representation is duplicated along the dorsal-ventral axis and adjacent pairs mirror each other. Mirror-imageduplication can be assessed using the visual field sign [20], defined as the sign of the cross-product of the gradients of the polar angle and eccentricity maps (Figure 1E-G). For details of the procedure, see Appendix A for the imaging method and Appendix B for the phase-encoding technique.

Layout of Areas

Figure 2 displays the retinotopic organization measured with the phase-encoding method for the entire visual cortex in inflated format. Based on the global pattern of retinotopy, we identified multiple retinotopic areas as possessing at least eccentricity maps. The polar angle map (Figure 2A, C) allowed us to reliably identify the borders V1v(d)/V2v(d), V2v(d)/V3v(d), V3d/V3A, and V3A/V7 as reversals in the polar angle and field sign map (Figure 2I, L). The foveal representations of V3A and V7 were displaced superiorly with the confluent foveal representation of areas V1, V2, and V3 (Figure 2E, G) [21]. As in other studies [22], the borders of other visual areas were placed with less certainty, since their angle maps were not clear. We designated the region just anterior to V3d as V3B [23], whose peripheral representation appeared to be located just inferior to the V3A foveal representation. We identified the region within the dorsal posterior limb of the inferior temporal sulcus as MT+, which featured a crude eccentricity map with a predominance of foveal representation inferiorly and peripheral representation superiorly [24]. We confirmed that this region mostly overlapped the middle temporal region, exhibiting a strong response to motion stimuli (Figure 2K, N). We refer to the large fan-shaped region between areas V3B and MT+ as LOc [25], which had a relatively clear eccentricity representation in the superior anterior direction from the confluent foveal representation [26, 27].

An enduring dispute exists regarding subdivision of the ventral occipital cortex anterior to V3v [10, 11, 22, 28, 29]. Here, we identified two areas, V4v and V8, after Hadjikhani et al. (1998)[30], stressing consistency not in the angle but in the eccentricity map of our data. Firstly, area V8 was determined as the small posterior region of the fusiform gyrus, which featured an eccentricity map with foveal representation anteriorly and peripheral representation posteriorly (Figure 2F, H), which roughly corresponds to the anterior part of hV4 (human V4) and the posterior part of VO (ventral occipital) [22, 31, 32]. Then, area V4v was determined as the region from the V3v/V4v border to the anterior limit of V8 (Figure 2B, D), which exhibited mirror-image representation (Figure 2I, L) and roughly corresponded to the posterior half of hV4 [31, 33, 34]. Notably, the entire region enclosing areas V4v and V8 has a simple angular map spanning the entire hemifield (Figure 2B, D), suggesting a single area instead of the two separated areas delineated here. However, if the hemifield region was defined as proposed in the definition of hV4, the region would have dual representations of eccentricity dimension (Figure 2F, H), resulting in loss of consistency in the eccentricity map.

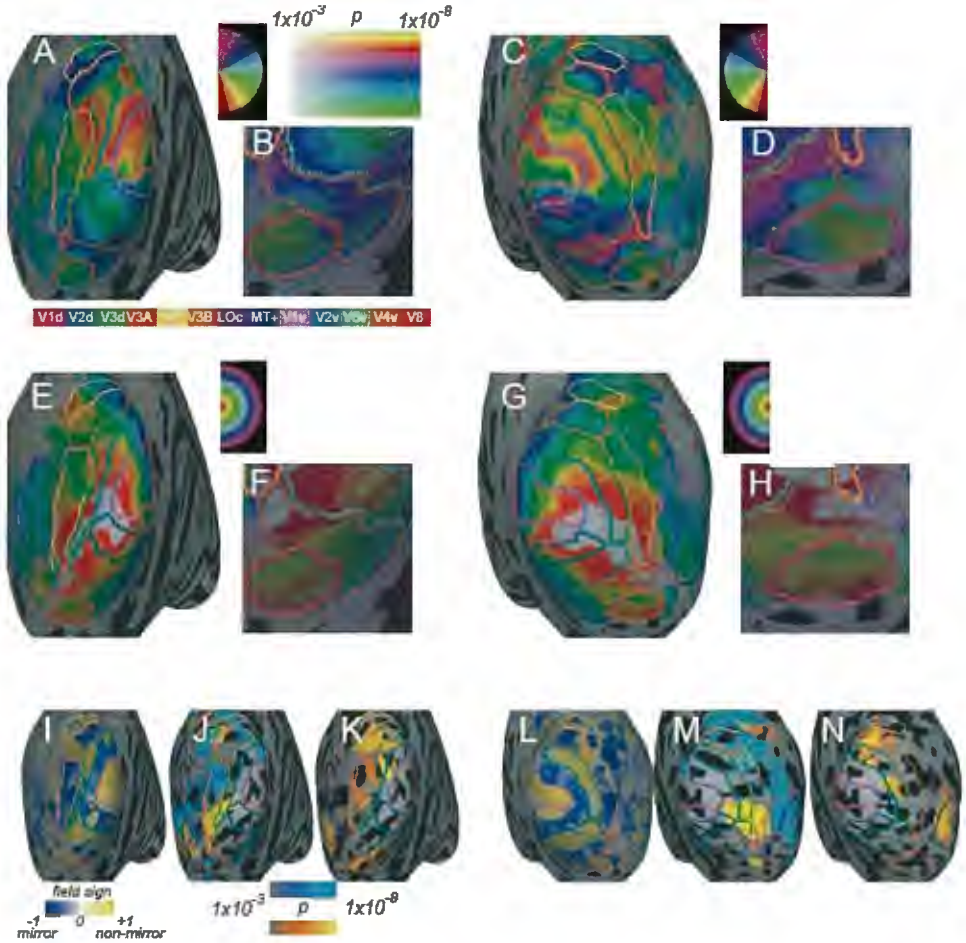

Figure 2. Locations of retinotopic areas, V1d/v, V2d/v, V3d/v, V3A, V3B, V7, V4v, V8, LOc, and MT+, in one subject's (S1) hemispheres and their relation to visual field representation (up to 16□ eccentricities) and motion-responsive regions of visual cortex. Information for the left and right hemispheres is shown in the left- and right-half regions of the figure, respectively. The colored lines on the inflated cortices indicate each area's border in accordance with the color code below A and B. (A, B, C, and D) Angular visual field representation measured by the phase-encoding retinotopy experiment. A and C display all data for visual cortex, while B and D zoom in on the posterior ventral region to better visualize the angular representation near areas V4v and V8. The color overlay on the cortex indicates the preferred stimulus angle at each cortical point, in accordance with the color code to the right of A or C. The more saturated the color, the higher the statistical significance of retinotopic activity, as shown in the rainbow-like color bar. (E, F, G, and H) Eccentricity visual field representation measured by the phase-encoding retinotopy experiment. Data are presented in the same format as in A, B, C, and D. (I and L) Field sign map computed from the angular and eccentricity maps. The blue code indicates mirror-image representation, while the yellow code indicates non-mirror-image representation. The greater the saturation of color, the stronger the degree of the mirror- or non-mirror-image (see the color bar on the bottom). (J and M) Foveal or peripheral representation measured by the experiment using the standard block paradigm. The yellow region indicates fMRI activity evoked by foveal stimulation, while the blue region indicates activity evoked by peripheral (16 °) stimulation (see the color bar on the bottom). (K and N). Motion-sensitive regions. The yellow region indicates fMRI activity evoked by expanding motion of a low-contrast concentric grating (see the color bar on the bottom).

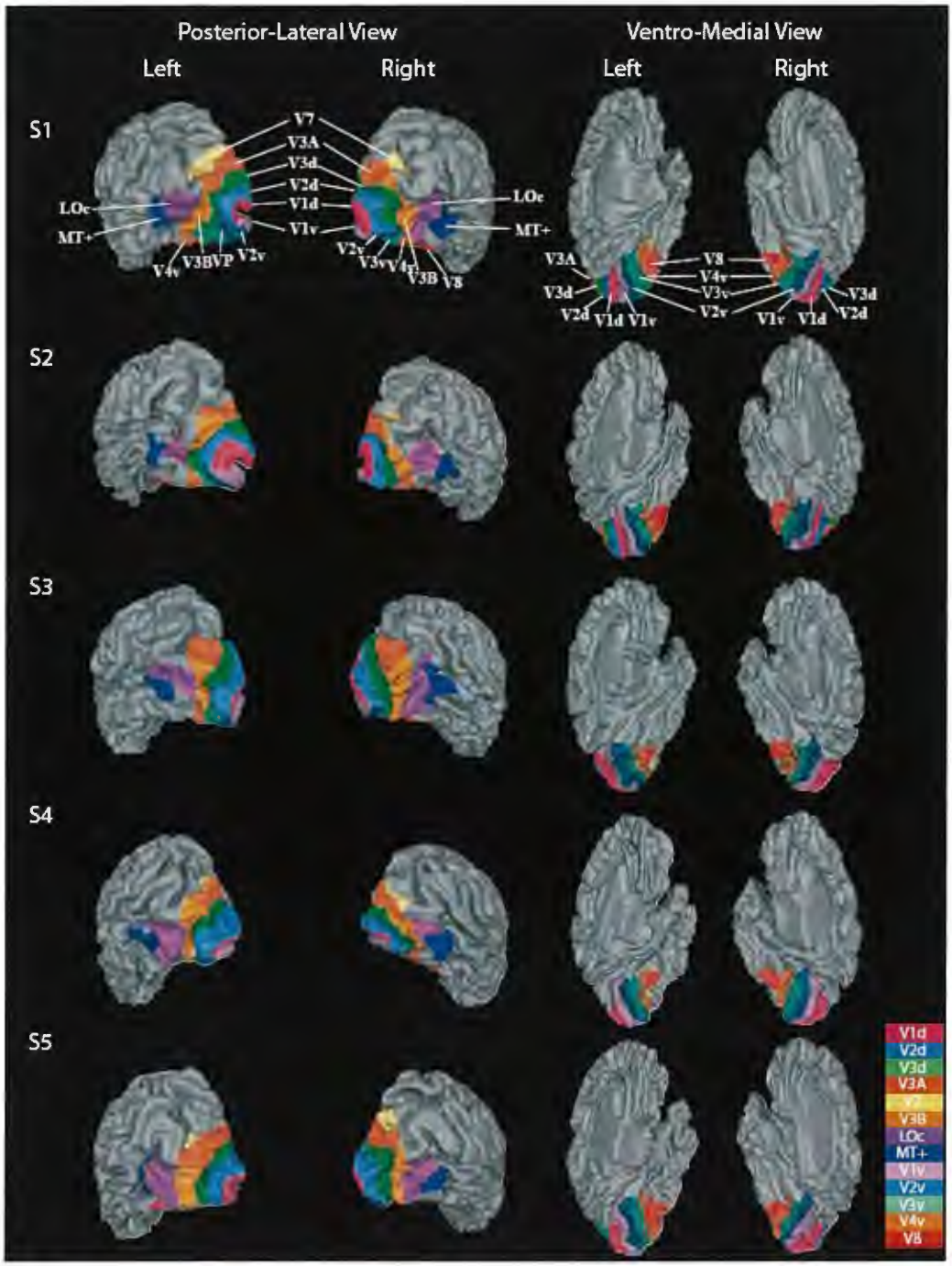

Figure 3. Locations of retinotopic areas of ten hemispheres determined from the visual field representation (e.g., Fig. 2). The five different rows show the layout of the areas from the five different subjects. The left two panels show the layout in the left and right visual cortex from a posterior lateral view (left), while the right two panels show them from a ventro-medial view. The icon on the bottom right indicates the relationship between color and visual areas.

Table 1. Talairach coordinates of visual areas

	Center of mass		
	X	Y	Z
V1d	8(2)	-91(4)	8(5)
V2d	13(4)	-95(3)	12(4)
V3d	18(4)	-92(3)	14(3)
V3A	17(5)	-87(3)	26(4)
V7	23(5)	-80(3)	28(5)
V3B	29(3)	-89(3)	9(4)
LOc	39(4)	-81(4)	7(4)
MT+	45(3)	-70(4)	4(4)
V1v	7(2)	-83(4)	3(4)
V2v	12(3)	-81(4)	-2(4)
V3v	19(3)	-78(4)	-4(3)
V4v	25(2)	-74(3)	-6(2)
V8	33(3)	-69(5)	-10(2)

Talairach coordinates specifying the center of mass of each area are listed. The columns labeled "Center of mass" show mean values (±SD) of the coordinates for ten hemispheres from five subjects.

Notably, along with localized areas, human visual cortex should contain retinotopic areas. For example, areas LOc and MT+ have been further subdivided (24, 26). New retinotopic areas have been reported just outside the zone defined here [31, 35-37].

Locations of Visual Areas in Talairach Space

We evaluated interindividual variability in Talairach space with respect to the position of a particular visual area, based on its center of mass (CM) [14]. Specifically, we began with the reconstruction of 10 cortical surfaces of both hemispheres from five subjects' anatomical scans (for details, see Appendix C). Next, we localized visual areas on each surface by the procedure described above. Figure 3 displays the locations of the areas on each of the ten reconstructed surfaces. Finally, the surface representation of each area was converted to a volumetric representation assuming that the cortical gray matter was 3 mm thick, and normalized into Talairach space by means of linear transformation (translation, rotation, and scaling) (for details, see Appendix D).

For each visual area, we computed the CM of its volumetric representations for 10 hemispheres in Talairach space. There was high intersubject variability in the CM for all visual areas (Table 1). The standard deviations of the X, Y, and Z coordinates of the CM ranged from 2 to 5 mm (mean, 3 mm), 3 to 5 mm (mean, 4 mm), and 2 to 5 mm (mean, 4 mm), respectively. These values were comparable to or greater than the thickness of the cortical gray matter, implying small overlaps between volumetric area representations from different hemispheres and thus the possibility of large inconsistencies between hemispheres in Talairach space.

The finding of ~4mm SD agrees well with previously reported values measured using various methods. In a positron emission tomography study (38), the average SD across areas other than V7, LOc, and V8 was 5 mm. In a cytoarchitectonic study [39], the average SD across V1 and V2 was 4 mm. In an fMRI study [40], in which the representative point was not the CM but the cortical point representing 12° eccentricity along the horizontal meridian, the average SD across V1 and the V2/V3 border was 6 mm.

Maximum Probability Maps

Although CM analysis suggests large positional inconsistency of visual areas in Talairach space, this analysis is limited in that evaluation is conducted using only one reference point of the volumetric area representation.

To examine potential inconsistency more directly and thoroughly, we created a 3D probability map of the visual areas, in which each voxel was associated with probabilities of occurrence for each of the areas [14, 15, 41-43]. The probability that a particular area was located there was determined for each voxel (1-mm cube) in Talairach space by assessing the frequency with which the volumetric representation of that area resided at each voxel across the ten hemispheres (for details, see Appendix D.).

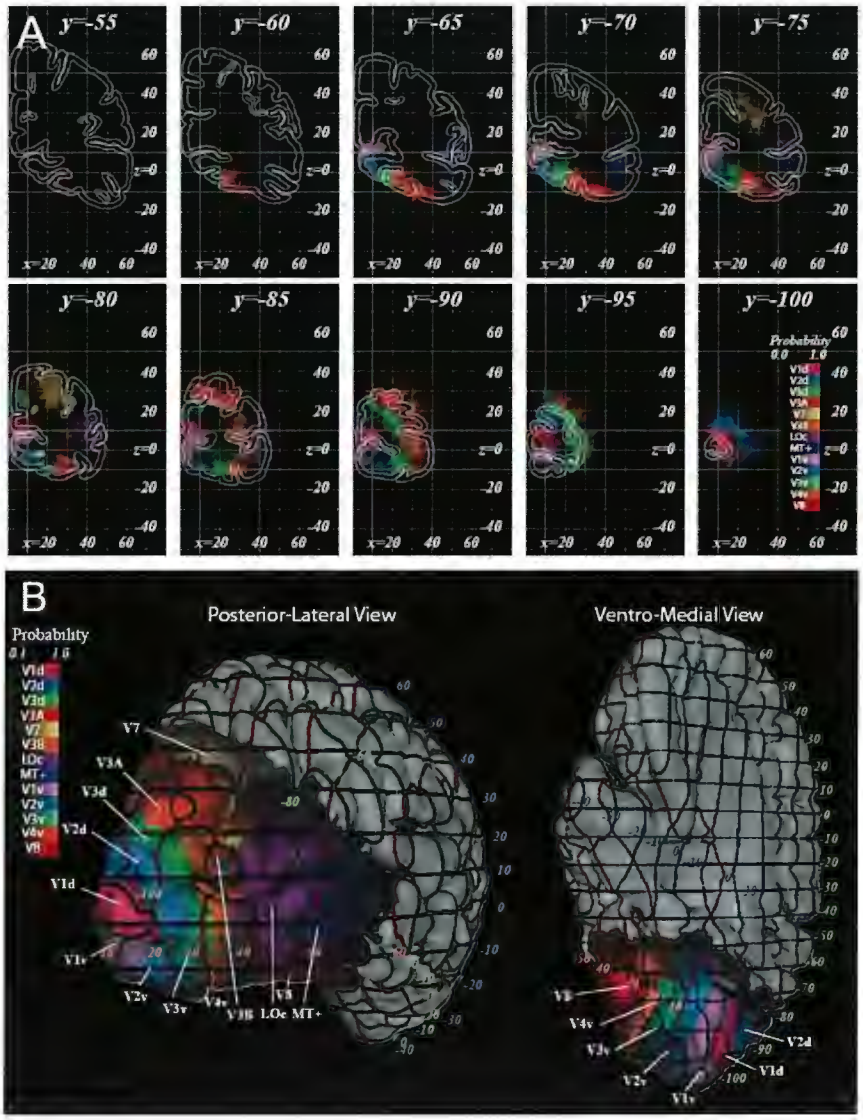

Figure 4. 3D maximum probability map of human visual areas in Talairach space. (A) Slice maps of visual areas V1d/v, V2d/v, V3d/v, V3A, V3B, V7, V4v, V8, LOc, and MT+ in Talairach space on serial coronal sections. The visual area with the most occurrences and its probability of occurrence (i.e., maximum probability) for each voxel are color-coded using 13 different colors and 10 brightness levels, respectively (see the color bar in the lower right-most panel), and are superimposed on the outline drawing of the Talairach brain showing the cortical gray matter. The probability of occurrence of a given area was calculated by dividing the number of overlapping hemispheres by the total number (n = 10) of samples, all of which were aligned into Talairach space using global linear transformations (translation, scaling, and rotation). The maximum value of the probability obtained across all voxels was 0.8. (B) Surface representation of the 3D maximum probability map of the areas from two different views. The visual area with the most occurrences and the maximum probability at the nearest neighbor voxel in Talairach space are color-coded on the Talairach brain surface running midway between the outlines of the cortical gray matter depicted in A. The color codes (see the color bar on the upper left) are the same as in A. The red, green, and blue lines on the surface indicate X, Y, and Z Talairach coordinates, respectively.

Since it is difficult to display all such multivariate volume data in only two dimensions, only essential data are graphically presented in Figure 4A and 4B in the form of a maximum probability map, in which each point has been color-coded according to the visual area that resided there with the greatest frequency (the maximum probability area) and brightness represents the probability that that area resides at that voxel. Regions of maximal consistency are shown with maximal brightness, while regions with minimal consistency are shown with minimal brightness. Figure 4A displays this information using the same coronal serial slices as the 1988 atlas of Talairach and Tournoux (1988), overlaid on the Talairach brain, the gray matter of which is outlined using white lines. The maximum probability area changes within the slices in the same hierarchical order as in individual hemispheres. This topographic pattern is clearly illustrated in Figure 4B, which shows the maximum probability map overlaid on the surface representation of the Talairach brain. Topographic preservation can be confirmed, except for the island-like V3 regions within V3B, by comparing the probabilistic map with the individual maps (Figure 3).

In contrast to the almost complete preservation of the topographic relations of the maximum probability areas, the probability maps of corresponding areas revealed substantial inconsistency. As can be seen to some extent in Figure 4A, the probabilistic volume for a corresponding area is rarefied and blurred so strongly that its extent is much wider than the thickness of the cortical gray matter. The strength of this tendency appears to vary among the visual areas, being strongest for area V7.

3. Retinotopic Organization within Visual Areas

As noted above, visual signal from the retina is locally processed in the visual areas with preservation of retinotopy. The basic question regarding such topographic processing concerns the possibility of its anisotropy across the retinotopic cortex, especially as regards the retinal eccentricity dimension. Since the central retina features a one- to two-thousand-fold higher density of retinal cones and ganglion cells than peripheral retina [44] and thus contains much fine-grained visual information, foveal and parafoveal signals are undoubtedly analyzed extensively in higher resolution. Indeed, such center-weighted analysis has been demonstrated physiologically in monkey visual cortex. The area of V1 devoted to representation of the central retina is much larger than that to peripheral retinal [8, 45, 46]; this is referred to as cortical magnification of central vision [47]. In addition, V1 neurons contributing to central vision have smaller receptive fields (RFs) than do those contributing to peripheral vision [48].

We investigated the cortical magnification and receptive field size of human lower areas across the cortex along the eccentricity dimension, by reanalyzing fMRI time series in the expanding annulus experiments. The analysis was performed not with the response phase mapping method but with a more elaborate method which took account of possible variations in waveform along the eccentricity dimension. This is illustrated with V3 as an example in Figure 5.

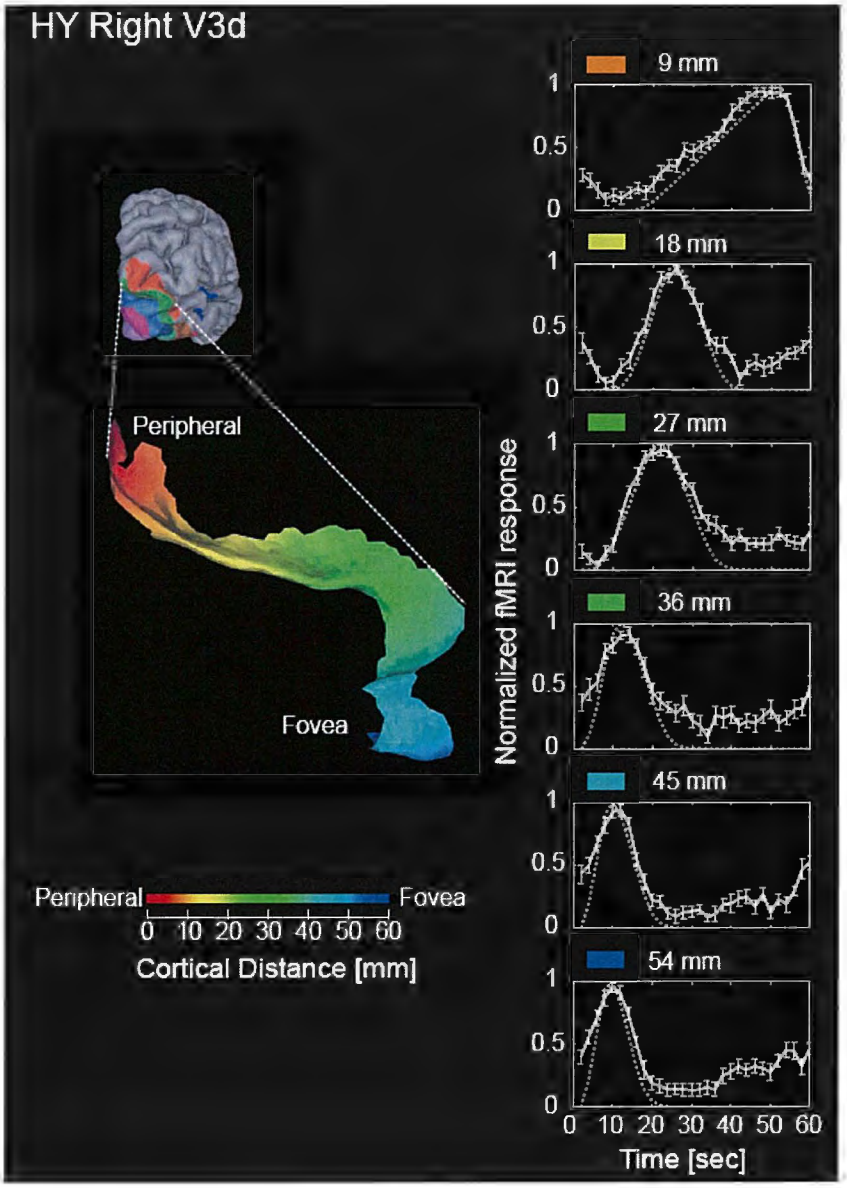

Figure 5. Isoeccentricity analysis of the retinal eccentricity mapping experiment. (Left) The cortical surface of V3 isolated from the right hemisphere of one subject. The color overlay on the cortex indicates the cortical distance measured from the superior edge representing 16°, in accordance with the color code at the bottom of the surface. Cortical bands of identical colors thus represent the same eccentricities. (Right) Each panel show one cycle of fMRI time-series (average of repeats) at each isoeccentricity band, when a checkered annulus expanded repeatedly from the central to peripheral visual field with a period of 60 s. Retinal eccentricity increases from bottom to top panels. Error bars denote SE across 5 subjects. The dotted smooth lines are the best fits obtained with a two-stage linear model (see the text).

Using a method we term isoeccentricity analysis (Appendix E) [49], we first divided the areal cortical surface into isoeccentricity bands based on the cortical distance from the peripheral 16° contour in the superior region of the area as shown in Figure 5 on the left, and

then separately pooled the fMRI responses evoked from different isoeccentricity bands. The right panels of Figure 5 compare the pooled fMRI time-series across the bands. As expected, fMRI activity progressed from inferior to superior as the stimulus ring moved from foveal to peripheral vision. Two important points should be noted concerning this finding. First, the peak of the waveform progressed more slowly across the fovea and parafoveal regions than the peripheral region, indicating that the RF centers of neurons representing the central visual field shift slowly, indicating higher cortical magnification for central vision. Second, the shape of the waveform changed markedly from peaked to broad with increasing eccentricity, indicating larger RF size for peripheral vision.

To obtain quantitative estimates of these RF characteristics, we constructed a two-stage linear model of the fMRI response, in which neuronal activation was first determined by spatial summation of the stimulus within a RF model, and it was then mapped onto the fMRI response via convolution with a hemodynamic impulse response [50]. The RF model has two parameters, RF center and size, and its sensitivity profile is approximately linear. The appropriate model parameters were then determined by a grid search technique. This procedure yielded good fit for the data, as shown in the right panels of Figure 5 (solid lines), and two reliable parameters, RF center eccentricity and size, could be extracted for areas V1, V2, V3, V3A, VP, and V4v from ten hemispheres.

Cortical Magnification Factor

Figure 6A plots the estimated RF center eccentricity for each of the lower areas as a function of cortical distance relative to the 8° point for ten hemispheres from five subjects. Although the data are somewhat scattered, the plots clearly show cortical magnification and suggest an exponential or logarithmic mapping between cortical position x and RF eccentricity E, which is a standard model for primate retino-striate mapping [51, 52]. We therefore fitted the data with an exponential function

$$E(x) = -(8+\sigma)\exp(x/A) - \sigma \tag{1}$$

where A and σ are constants. The data were fit well by the retino-cortical mapping function (smooth curves; least-squares fit, $R^2 = 0.77 \sim 0.85$). Table 2 shows the parameter values and their confidence intervals from the curve fits. No significant differences were found in two parameters among the areas. Superimposition of the mapping function also reveals no clear differences in the mapping functions among the areas, although small deviations from the others were demonstrated for V3A and V3v in the opposite directions (Figure 6B). The mean values of the parameters A and σ among the six areas were 22.9 (SD = 4.2) and 2.4 (SD = 1.2), respectively. A larger variance was obtained for σ mainly because we could not measure eccentricities near the fovea.

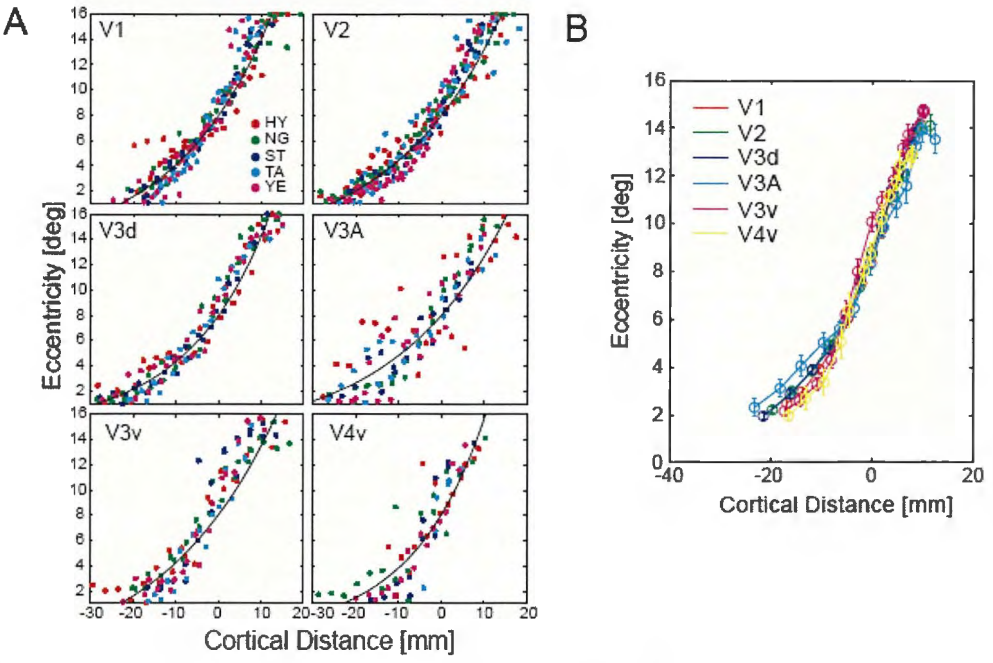

Figure 6. Retino-cortical mapping functions of human visual areas V1, V2, V3, V3A, VP, and V4v. (A) Each panel shows the visual field eccentricity of RF center in each area as a function of cortical position. The position is specified by the cortical distance from the point representing 8° eccentricity; negative and positive values indicate respectively more central and peripheral positions with respect to the origin. For each area, the mapping functions from 10 hemispheres were shifted to match at the origin. The smooth curves are the exponential functions (Eq. 1. in the text) that best fit the data. (B) Superposition of the mapping functions of different visual areas. Each symbol type represents the function for each visual area. Error bars denote SE across 5 subjects. For the data for A, cortical distances were grouped into bins and the average eccentricity within each bin was computed.

Based on the curve fits, a principal measure of retino-cortical mapping, called the cortical magnification factor and introduced by Daniel and Whitteridge (1961), can be computed. The magnification factor M is defined as the distance in cortex (in millimeters) dx devoted to representation of a step of 1° in visual field eccentricity dE and thus corresponds to the derivative of the inverse function of Eq. (1)

$$M(E) = \frac{dx}{dE} = \frac{A}{E+\sigma} \text{ [mm / deg].} \tag{2}$$

Consequently, the cortical magnification factor M can be obtained using Eq. (2) from the two estimated parameters σ [deg] and A [mm]. Notice from Eq. (2) that foveal M is given by A/σ and thereby the parameter σ represents the visual field eccentricity at which M becomes half of the foveal value. The significance of the parameter A is made clear by rearranging Eq. (2) to

$$dx = A\frac{dE}{E+\sigma}. \tag{3}$$

The quantity A is thus the cortical distance moved per percent change in eccentricity when the eccentricity E is much larger than the value of σ.

Table 2. Parameter estimates of retino-cortical mapping function

	A	σ
V1	22.6 (18.0, 27.2)	2.9 (0.9, 5.0)
V2	25.6 (21.6, 29.7)	3.0 (1.5, 4.5)
V3d	18.7 (16.3, 21.1)	0.9 (-0.1, 1.9)
V3A	26.0 (17.0, 35.0)	1.9 (-1.0, 4.9)
V3v	27.2 (18.0, 36.4)	4.3 (0.5, 8.2)
V4v	17.0 (10.6, 23.5)	1.5 (-1.5, 4.5)

The best fitted constants of Eq.1 and Eq. 2 and 95% confidence interval (in parentheses) are listed for each area.

By substituting the parameter estimates (Table 2) into Eq. (2), we could obtain the cortical magnification factor M and its reciprocal M^{-1} as a function of visual field eccentricity. Figures 7A and 7B show the relationship between M and M^{-1} and eccentricity for each of the six areas, respectively. The values for the fovea and 16° peripherally are given in Table 2. The value of M was ~1 mm/deg with M^{-1} of 40 - 60 min/mm in peripheral cortex, and increased by a factor of 5 - 20 to 6 - 21 mm/deg in foveal cortex, with M^{-1} of ~ 3 min/mm. In calculating foveal M using the average A and σ among the areas, we obtained a value of 9.5 mm/deg.

The cortical magnification factor of monkey visual cortex has been extensively studied by electrophysiological recording [8, 9, 45, 46]. For humans, several studies have estimated it using fMRI [17, 40, 53, 54], visual evoked potential recording [55], subdural electrode recording [56], lesion imaging [57], and psychophysical methods [58, 59]. Figure 7C and 7D compare our V1 data with those obtained by some of these studies. The cortical magnification factor M we measured is in the range obtained for monkeys and humans obtained with the various methods noted above. Among other studies, the present findings (Table 2) agree remarkably well with the fMRI study by Dougherty et al (2003)[40], who have, for example, estimated M = ~4 mm/deg at 3° in V1 and the parameters A and σ of the M function (Eq. 2) to be A ~= 20 – 30 mm and σ ~= 2.5 – 3.5 for areas V1, V2, and V3.

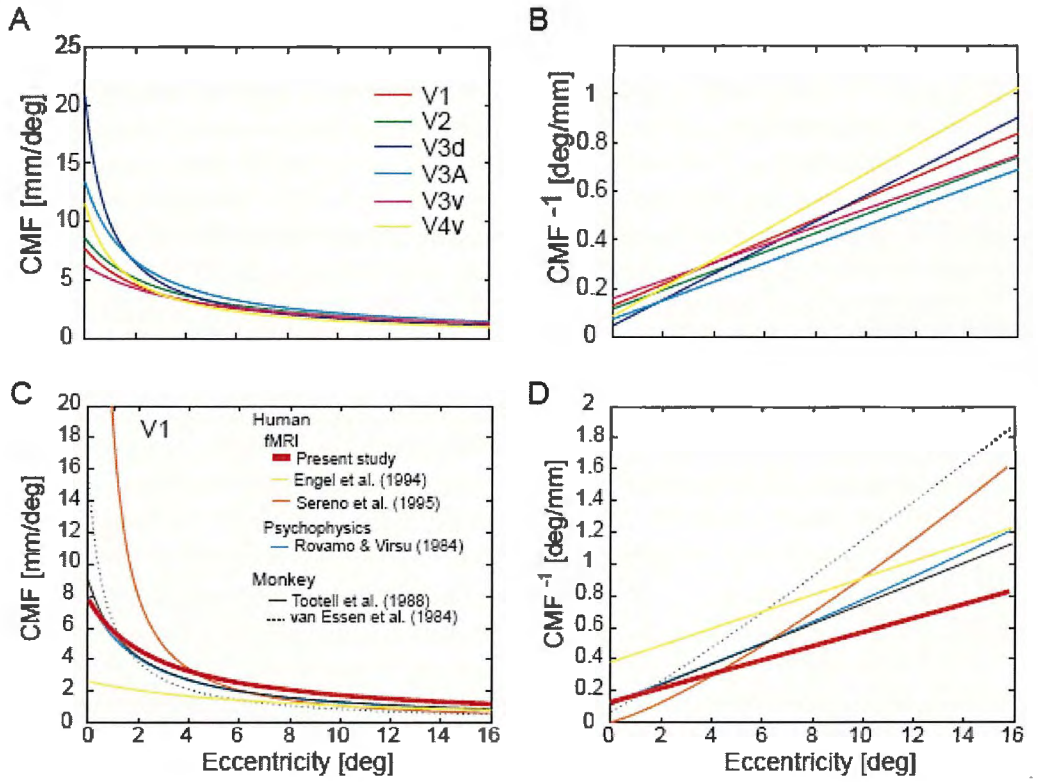

Figure 7. The relationship between cortical magnification factor M or its reciprocal M^{-1} and retinal eccentricity. (A) M in human V1, V2, V3, V3A, VP, and V4v as a function of eccentricity. This function is obtained by substituting the parameter estimates (Table 2) of the retino-cortical mapping model (Figure 5) into Eq. (2). Each symbol type represents the function of each visual area. (B) Similar plots for M^{-1} as in A. (C) Comparison of M in human and monkey V1 across studies. The red thick line displays the data from this study, compared with results for humans from fMRI studies of Engel et al. (1994) (19)and Sereno et al. (1995) (53)and from psychophysical experiments of Rovamo and Virsu (1984), as well as results for monkeys, including a C14-2 deoxy-D-glucose (2DG) uptake study by Tootell et al. (1988) (46)and the single-unit recording study by Van Essen et al. (1984)(45). The function of Engel et al. (1994) is based on the estimate by Beard et al. (1997)(58) using Engel et al.'s data. (D) Similar plots for M^{-1} as in C.

Receptive Field Size

Figure 8 plots estimated RF sizes for each of the six areas as a function of visual eccentricity, and highlights two important points. The first concerns the relation between RF size and eccentricity. For all of the areas, RF size monotonically increased by a factor of about 3 or more from 2° central to 14° peripheral visual field. The rate of increase was higher for areas V3A, VP, and V4v than for V1, V2, and V3. The second important point concerns the difference in absolute size between areas. In contrast to cortical magnification factor, there was a clear areal difference in RF size over the range of eccentricities. Importantly, RF became progressively larger with ascension of the visual cortical hierarchy from V1 to V4v.

The differences among V1, V2, and V3 were relatively small, and their RF sizes at 4° and 10° eccentricity were ~2° and ~6° in radius, respectively. The RF size of VP was larger by a factor of 1.5 – 2 than those of V1/V2/V3. The RF sizes of V3A and V4v were substantially larger than those of the lower areas, and approached 7° or more in radius at 4° in the paracentral visual field.

The enlargement of RF size with increase both in visual eccentricity and in the hierarchical level of visual areas is in line with the data reported for monkey visual areas [48]. For humans, there are two fMRI studies reporting such enlargement [60, 61], though these studies did not measure the absolute RF size. More recently, Yoshor et al. (2007) directly measured RF size by subdural recording and found that the RF width of a cortical point in V1/2 located 10 – 20 mm (eccentricity ~2° - ~6° from Figure 6) from the occipital pole is ~2°. This value is, at most, half that we measured (Figure 7), suggesting that the RF size estimated by fMRI does not directly reflect the size of classical receptive fields. This point will be considered in the next subsection.

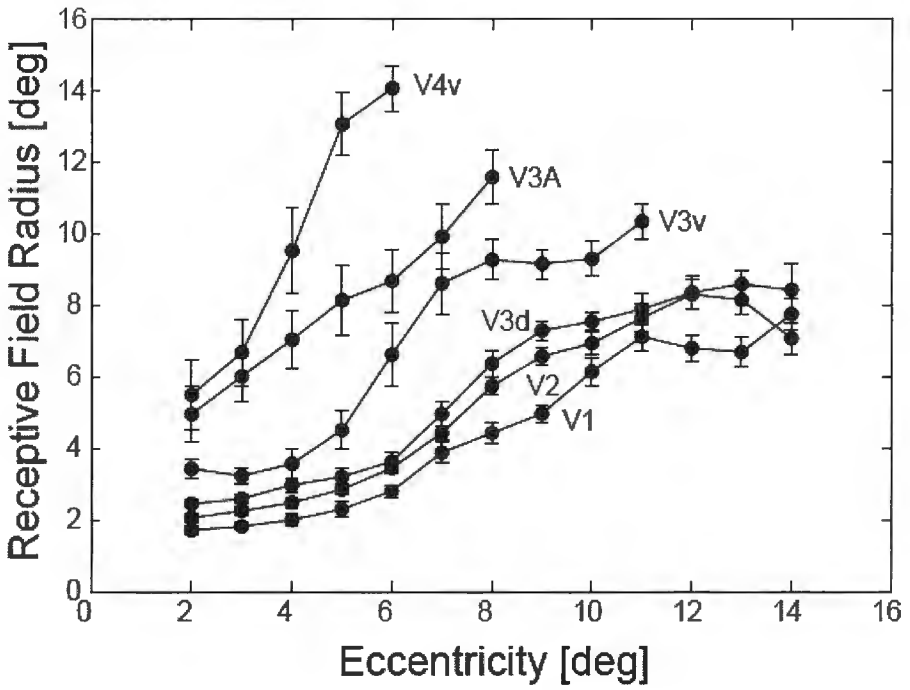

Figure 8. Relationships between receptive field size and retinal eccentricity for human V1, V2, V3, V3A, VP, and V4v. Error bars denote SE across 5 subjects.

Point Spread

We have thus seen that both the reciprocal of cortical magnification factor M^{-1} (the distance moved through the visual field corresponding to a 1 mm distance along cortex) and RF size increased with eccentricity. The relationship between M^{-1} and RF size is of fundamental significance in understanding the functional organization of the retinotopic areas. Hubel and

Wiesel (1974) first investigated this relationship in monkey V1. They found that M^{-1} increased with eccentricity in strikingly parallel fashion with RF size and scatter, and that, independent of eccentricity, a movement about 2-3 mm along the cortex was needed to get out of one region of visual field to enter an entirely new one. To put it another way, the point image or point spread, defined as the cortical region activated by a point stimulus, is constant at 2-3 mm across cortex. They argued that point spread can be considered indicative of the machinery required for analysis of the corresponding visual space, since its size is comparable to an ocular hypercolumn or an orientation hypercolumn, and that the machinery may be roughly uniform over the striate cortex. In this fashion, point spread provides information on the functional unit of local analysis of a finite region of the visual field.

To test whether a functional organization similar to that in monkeys exists in humans, we performed an analogous analysis for the retinotopic areas, based on estimated cortical magnification factor and RF size. Point spread could be calculated by multiplying RF size by the cortical magnification factor, since it corresponds to the image of RF on the cortex (Figure 9A) [62]. Figure 9B shows the relationship between point spread and visual field eccentricity. There appears to be an eccentricity-dependent variation in point spread, indicating deviation from exact parallelism between RF size and M^{-1}, since M^{-1} is modeled to increase in linear fashion (Figure 7B), whereas RF size increases in nonlinear fashion with eccentricity (Figure 8). However, because the variation was not large and no clearly defined trends could be established, the point spread may be constant along cortex, independent of eccentricity. Importantly, point spread became larger along the cortical hierarchy, as does RF size. The point spread radius averaged across eccentricities was 8.9 (SD=1.7) mm for V1, 11.8 (2.0) mm for V2, 12.2 (1.6) mm for V3, 15.5 (3.8) mm for VP, 22.6 (7.9) mm for V4v, and 26.8 (4.8) mm for V3A, in ascending order.

The near constancy of point spread suggests that, as for monkey striate cortex, human retinotopic cortex may be organized uniformly into an array of functional units, each of which analyzes visual information for a certain portion of visual space. Regarding the size of functional units, the estimated point spread of V1 was about 9 mm, and larger by a factor of ~10 than that of monkey V1 (8). We note, however, that this comparison is made difficult by methodological differences between our fMRI study and monkey single-unit electrophysiological recoding studies. Although fMRI signals reflect metabolic and vascular responses to neural activity, in particular changes in blood oxygenation and flow, their relationship to electrophysiological activity remains poorly understood [63]. Interestingly, the results of our measurement were comparable to those obtained by optical imaging based on intrinsic signals (IOS) [64], which detect blood-related signals, as fMRI does [65]. As suggested by the IOS study of Grinvald et al (1994), the large point spread of V1 detected by functional imaging may reflect long-range lateral interactions between the distinct functional units over the classical RF [66].

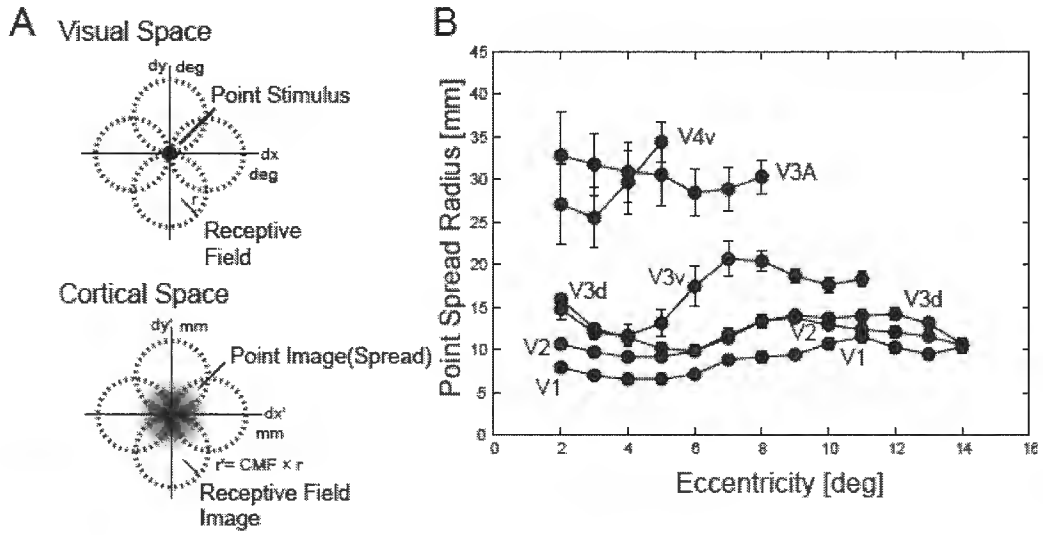

Figure 9. The concept of cortical point spread and its relationship to eccentricity (A) The left panel shows examples of the most remote receptive fields (dotted circles) of neurons activated by a given point stimulus. The right panel shows images of receptive fields (RF) on cortex (dotted circles) whose size can be computed by multiplying RF size (deg) by cortical magnification factor (mm/deg) at a given cortical point. The gray zone forms inside the center of the RF images and thus contains the neurons activated by the point stimulus. The gray zone is thus exactly the point spread, which is defined as the total area of cortex activated by a point stimulus. Consequently, the size of point spread corresponds to that of the RF image. (B) The point spread radii of human V1, V2, V3, V3A, VP, and V4v as a function of retinal eccentricity. Error bars denote SE across 5 subjects.

It is unclear what produces the enlargement of point spread with hierarchy level in extrastriate visual areas. Two factors relevant to their functional organization can be suggested. The first is the possibility of enlargement of their functional units themselves, which are comprised of multiple modules representing different functional domains such as the orientation hypercolumns of V1. The functional unit may become larger because the modules contained may increase in number to represent more functional domains. The second factor is the possibility of growth of the long-range lateral network between units, as found between V1 and the inferior temporal (TE) cortex of monkeys [67].

4. Retinotopy-Based Analyses of Visual Cortical Processing

Knowledge of retinotopic organization is important not only in itself, it also provides essential information for analysis and interpretation of functional activity in retinotopic cortex. In the previous section, we have already seen that findings from retino-cortical mapping enable employment of isoeccentricity analysis of phase-encoded activity to assess cortical point spread. In this section, we will summarize some of our studies that have employed similar retinotopy-based analyses.

Analysis of Visual Contextual Effects

Surround suppression: Retinotopy-based analysis is useful for investigating the neural substrates of visual contextual effects. Visual contextual effects refer to the change in perception of a visual stimulus caused by remote stimuli. One of the most representative of these phenomena is surround suppression, in which the perceived contrast of a test grating is reduced when similarly oriented and spaced surrounding gratings are presented nearby it [68, 69]. Neural correlates of surround suppression can be explored utilizing retinotopy, by first localizing the cortical regions that represent the test grating and then testing whether fMRI activities in the regions are correlated with perception. Isoeccentricity analysis does this in rigorous fashion using eccentricity-cortical mapping (Figure 5) when the stimulus can be specified by the eccentricity dimension alone. Based on this, we have investigated the neural correlate of surround suppression and found strong evidence for it in V1 and V2 [70, 71]. We also found an antagonistic pattern of response modulations between the test and surround region, suggesting that lateral interaction could be antagonistic between them. These findings confirm those of studies that have shown suppressive interaction among nearby stimuli in human early visual areas [72-74].

Bilateral contextual modulation: The existence of surround suppression in V1 suggests that some global feature integration begins at the earliest stage of the visual cortical hierarchy. However, it remains unclear how much remote space can be integrated. It is generally assumed that, in a bottom-up visual hierarchy, dissociated representations of an object located across the visual vertical meridian are combined only in higher visual areas in which the receptive fields of neurons are large enough to cover ipsilateral as well as contralateral visual hemifields. However, given the existence of massive feedback connections from higher areas targeting early visual cortex and reports of their contribution to contextual modulation [75, 76], it might be expected that early visual areas contribute to more global feature integration than previously thought, even beyond dissociated representations of visual hemifields.

To test this intriguing hypothesis, we performed block-design human fMRI experiments in which circular visual patterns aligned with various configurations were used (77-79). Each pattern consisted of centrally foveated quarter arcs, each of which was located in one quadrant of the visual field (Figure 10A), which permitted precise localization and anatomical separation of an early cortical representation of an arc from others. Using isoeccentricity analysis, we investigated whether the retinotopic neural responses corresponding to a target arc were modulated by other arcs presented in nonassociated visual fields when such elements were perceptually linked into a whole structure. Figure 10B shows spatiotemporal fMRI activity in right V1d for localize, target arc alone, and target plus context conditions. The spatiotemporal plot clearly shows that retinotopic responses to the target arc were significantly enhanced when another arc was simultaneously presented at the point-symmetrical position in the nonassociated visual field quadrant. This finding is convincing evidence that contextual effects involve feedback from higher areas, since there are no direct callosal connections that permit such interhemispheric contextual modulation. Early visual areas as well as higher ones may thus play more essential roles in perceiving the unity of the real world than previously thought.

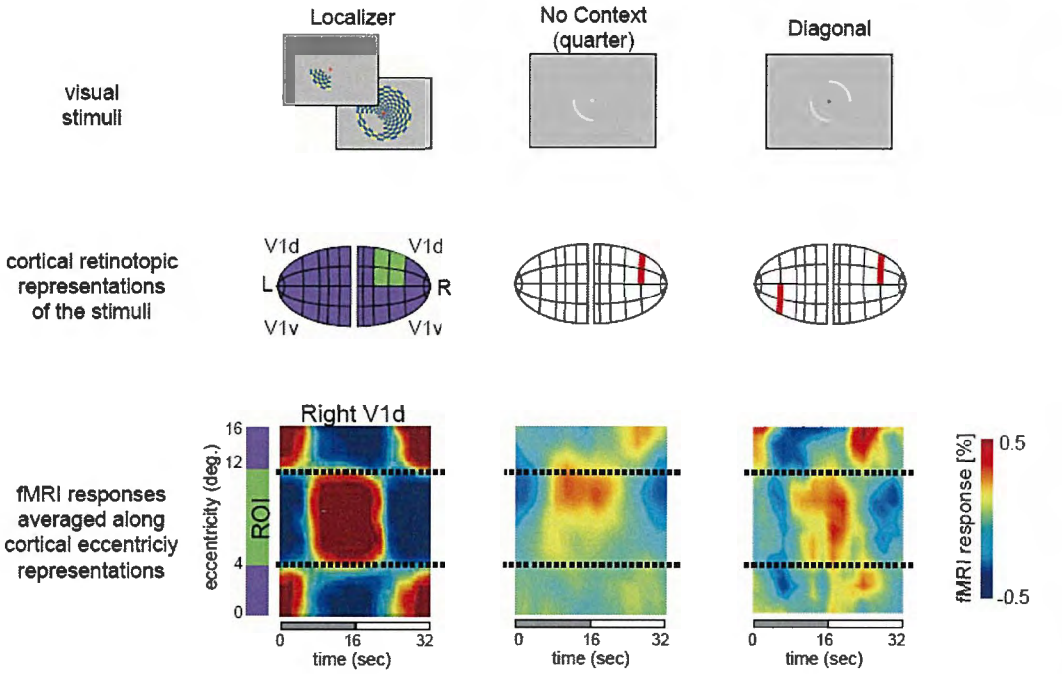

Figure 10. Interhemispheric contextual modulation in V1. [Top Row] Visual stimuli. (Left) Localizer. We localized the cortical sub-regions representing a portion of the visual field where the target stimulus was presented in the subsequent main experiments (4-12 deg in eccentricity in the lower-left visual quadrant). This localization was performed for V1d, V2d, and V3 on the right cerebral hemisphere of each participant using a checkerboard pattern spanning the target zone. (Middle) No context stimulus. In the No Context condition, we presented the target quarter arc alone within the pre-defined lower-left visual field quadrant. (Right) Context stimulus. In the Context condition, we presented the target arc with another arc in the non-associated visual field quadrant so that the two arcs were globally completed into a complete annulus. Note that although these annular stimuli (middle and right panels) differed in global configuration, their lower-left portions were completely identical, and were represented retinotopically within the pre-defined regions in early visual cortex. [Middle Row] Each icon shows the cortical retinotopic representation for the corresponding stimulus in the top row panels. [Bottom Row] Representative spatiotemporal fMRI activation patterns for different eccentricities in the right V1d of one representative participant are shown as images with an interpolated pseudo-color format indicating the magnitude of fMRI responses. In these spatiotemporal plots, the vertical axis represents eccentricity (top-peripheral and bottom-foveal) and the horizontal axis represents time per period of stimulus presentation (16 sec stimulus presentation and 16 sec rest). Each horizontal trace of the 2D plot shows the averaged fMRI time course within a given isoeccentricity region. (Left) fMRI response patterns evoked by the localizer. (Middle) fMRI response patterns evoked by a quarter arc presented alone within the lower-left visual field quadrant (No Context). (Right) fMRI responses evoked by the target stimulus with the context leading to completion of the entire annulus.

Inverse Mapping: Representation of Brain Activities in the Visual Field

In isoeccentricity analysis, fMRI activity is collapsed across the polar dimension to improve signal-to-noise ratio. However, it is also possible not to perform such pooling and to analyze and represent fMRI activity in both the eccentricity and polar angle dimensions, that is, in the

visual field as is. We have produced software that can map fMRI activity from the retinotopic cortex to the visual field [80]. Using this inverse mapping, we can create movies of fMRI activity in the visual field for a given retinotopic area while subjects view a stimulus movie. Figure 11A displays shots from such activity movies for the phase-encoding experiments. As illustrated in Figure 11A, this technique permits direct comparison of brain activity with visual stimuli in a common reference frame. Their topographic relation can thus be captured intuitively and easily analyzed, in evaluating hypotheses linking brain activities and visual perception [81, 82].

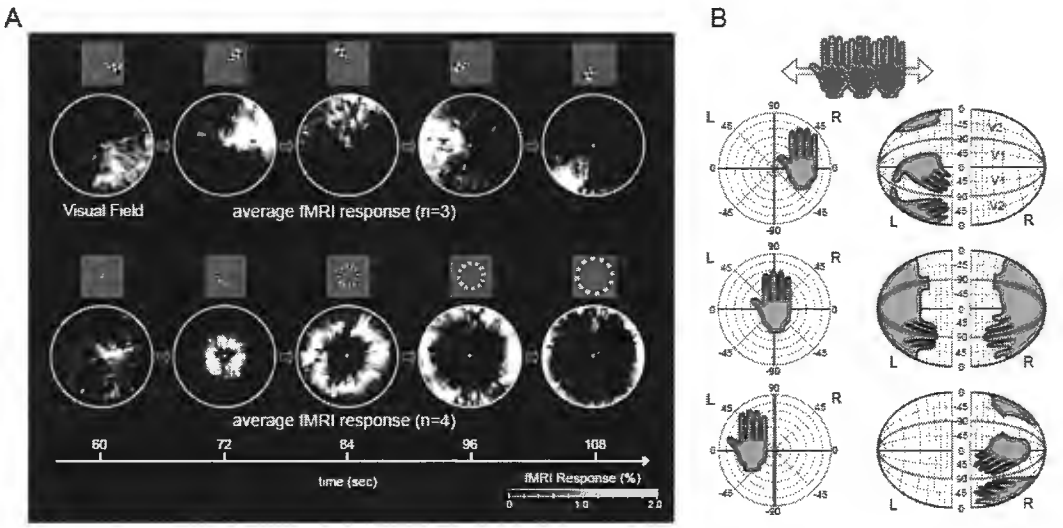

Figure 11. Inverse mapping: representation of brain activities in the visual field. (A) Snapshots from fMRI activity movies for the phase-encoded stimuli in V1 represented in the visual field coordinate (time for stimulus presentation shifts from left to right). [Above] fMRI activities for the rotating wedge stimulus. The wedge rotated along the central fixation point counter-clockwise from slightly below the right horizontal meridian. The circular image snapshots represent the corresponding fMRI response patterns obtained at each stimulus presentation period inversely mapped in visual field coordinates and averaged among three subjects. Interpolated pseudo-colors represent the magnitude of fMRI responses as shown in the indicator below. [Below] fMRI activities associated with the expanding annulus stimulus. The annulus expanded from central fixation to the peripheral visual field. The circular image snapshots represent the corresponding fMRI response patterns obtained at each stimulus presentation period and averaged among four subjects. (B) Cortical retinotopic representations of the right hand. [Left Panels] The position of the right hand in the visual field. [Right Panels] The cortical retinotopic representations of the right hand corresponding to the position shown in the left panels. When the right hand is entirely located within the right (or left) visual hemifield, it is represented only within the left (or right) cerebral cortex (top or bottom row). Yet, when the right hand is located across the vertical visual field meridian, it is represented separately in each cerebral hemisphere, forming fragmented imprints (middle row). As demonstrated in these panels, imprints formed by objects on the cerebral cortex change remarkably from the way that they appear, depending on subtle changes in spatial position in the visual field.

It should be noted that such comparison is not easy with standard forward mapping, since the topology of activation on retinotopic cortex is often quite different from that of stimuli due to singularities in retinotopy (split between left/right hemispheres and dorsal/ventral

cortices, mirror-image duplication between areas, nonlinear scaling for different eccentricities), even if the stimulus configuration is simple [79, 83]. This is nicely illustrated in Figure 11B, which shows the retinotopic representation of a hand in V1 and V2.

Another advantage of inverse mapping is that it can be applied to comparison or integration of functional data among individuals. As shown in the first section, linear Talairach registration cannot actually normalize individual differences in locations of visual areas. Nonlinear or surface-based methods based on anatomical structures exhibit significantly better performance in this regard [2], though they have the inherent limit that no clear structure-function relationships are found in most visual areas. Inverse mapping provides an ideal method of normalization of individual differences not only in the layout of visual areas but also retino-cortical mapping within each area.

Conclusion

Measurement of retinotopy has significantly advanced our understanding of the functional organization of the human visual cortex. Not only has it revealed how multiple visual areas are distributed over the cortex for repeated analysis of the entire visual field, it has uncovered how populations of neurons form an array of functional units, each of which analyzes a finite region of the visual field. The human visual cortex appears to analyze a visual scene with functional units having common machinery within a given area, but with more elaborate machinery as the visual hierarchy is ascended. Furthermore, measurement of retinotopy has provided strong clues to elucidation of the interaction between the functional units that underlie visual contextual effects.

While much of visual cortex is composed of visual field maps, there is also emerging evidence for visual category or feature-specific maps. How do these two types of organization coexist on the cortex and cooperate in visual function? Although the answer to this question is far from certain, as only a few studies have explored the relationship between them (84, 85), the findings described here provide basic data of use in obtaining it.

Acknowledgements

Sections 2 and 3 of this chapter are based on parts of H. Yamamoto's doctoral dissertation [86]. A portion of section 4 is based on parts of H. Ban's doctoral dissertation [87]. This work was supported by the 21st Century COE Program (D-2, Kyoto University) and Global COE Program (D07, Kyoto University), a Grant-in-Aid for Young Scientists (B) of the Ministry of Education, Culture, Sports, Science, and Technology of Japan, and the Strategic Information and Communications RandD Promotion Programme (SCOPE) of the Ministry of Internal Affairs and Communications of Japan.

Appendix A. Imaging Methods

Structural and functional MR measurements were carried out using a standard clinical 1.5 Tesla scanner (General Electric Signa NV/i, Milwaukee, WI). Before the experimental scans,

high-contrast structural images of the whole brain were recorded as a standard brain once for each subject using a T1-weighted three-dimensional (3D) SPGR [echo time (TE) = 3.0 ms, repetition time (TR) = 56 ms, flip angle (FA) = 55°; excitations (NEX) = 1, voxel size (VS) = 0.781 × 0.781 × 1.4 or 0.938 × 0.938 × 1.4 mm]. A standard quadrature head coil was used for radiofrequency transmission and reception. This standard structural volume was used for reconstructing the brain surface (Appendix C).

For each subject, three types of images were obtained on each scan day, with a standard flexible surface coil placed at the occipital pole. First, structural images for anatomical registration were acquired using a T1-weighted Inversion Recovery 3D Fast SPGR [TE = 2.7 ms, TR = 6.0 ms, inversion time (TI) = 600 ms, FA = 15°; NEX = 1, VS = 0.781 × 0.781 × 1.4 mm]. Second, a set of 16 or 17 adjacent high-resolution anatomical slices was obtained using a T1-weighted spin echo [TE = 9 ms, TR = 420 ms, NEX = 2, VS = 0.781 × 0.781 × 4 mm]. These slices included the occipital, posterior parietal, and temporal lobes, oriented roughly parallel with or perpendicular to the calcarine sulcus. Finally, multiple functional scans were obtained in the same slices as these oblique anatomical slices while the subject viewed visual stimuli, using T2*-weighted two-dimensional gradient echo, echo planar imaging [TE = 50 ms, TR = 2000 ms, FA = 90°, VS = 1.563 × 1.563 × 4 mm]. For each scan, 180 functional images depicting blood-oxygen-level-dependent (BOLD) contrast (Ogawa, et al. 1992) were collected for each of the slices. Head movement was minimized using a custom-made head fixation device, which is best described as a screw-operated clamp that holds the temporal region of the head.

Appendix B. Localization of Retinotopic Areas Using fMRI

The locations of retinotopic visual areas on each individual's cortical surfaces were identified with fMRI, using standard techniques for measurement and analysis of retinotopic organization [53, 88, 89]. The retinotopic map was constructed using a phase-encoding technique in which receptive field centers are temporally coded using polar coordinates [19]. The eccentricity component was measured while the subject viewed a checkered annulus (2° width; Figure 1A) that expanded from the fovea to 16° peripherally over 50 s and then disappeared for 10 s. The polar angle component of the map was measured by carrying out fMRI while the subject viewed a wedge-shaped checkered pattern (24° center angle; Figure 1B) rotated counter-clockwise around the fixation point, making one rotation in 60 s. Each stimulus underwent color (black/white, red/green, blue/yellow) pattern reversal (1 Hz) and was presented in six cycles, evoking a periodic response at a given point on the retinotopy map, whose corresponding position in the visual field was encoded in the phase of the response. The response phase for each of the eccentricity and polar angle components was computed by Fourier analysis and mapped onto the cortical surface after correction for hemodynamic delay (Figure 1C, D; Figure 2). The statistical significance of retinotopic activity was determined by Fourier F-test [90]. We further calculated the visual field sign [20] from the polar angle and eccentricity maps. After the gradient vectors of the angular and eccentricity representation were computed at each cortical point, the field sign was determined as the sign of the cross-product of the two gradients and mapped onto the cortical surface (Figure 1E-G).

Two other series of fMRI experiments were conducted to help determine localization. First, foveal and peripheral representations were localized (Figure 2J, M) using a block design in which foveal and peripheral (16°) dot stimuli were presented in alternating blocks of 16 s each, interleaved with blank periods or not interleaved. Second, motion-sensitive regions were localized (Figure 2K, N) using a block design in which expanding motion of a low-contrast concentric grating was presented in blocks of 16 s interleaved with blank periods. The statistical significance of these activities was determined by the Fourier F-test.

Appendix C. Cortical Surface Reconstruction

Individuals' cortical surfaces (Figure 3) were reconstructed using the standard structural volume for each hemisphere. We generated a surface lying approximately in the middle of the gray matter using a method that was a hybrid of volume segmentation [91] and surface deformation [92]. First, the voxels that belonged to the cortical gray matter were segmented from the rest of the volume using mrGray software (93). mrGray enabled us to identify the white matter, cerebrospinal fluid (CSF), and three layers of gray matter. The segmented gray matter was approximately 3 mm thick and the first, second, and third layers were positioned in that order relative to the white matter. From the output, we constructed a segmented volume whose voxels were numerically labeled as white matter (label = 200), CSF (0), or the first (150), second (100), or third (50) layer of gray matter. The segmented volume was then slightly smoothed using a 3D Gaussian filter with a SD of 1 voxel. The resultant volume was smooth and noiseless enough that we were able to minimize any non-biological irregularities that might have arisen in subsequent processing. Next, a surface representation was created for the gray-white matter boundary. At this point, we did not create the surface for the middle of the gray matter, in order to minimize topological defects, in particular bridges between cortical sulci. We then computed a concrete average voxel value for the first gray matter layer in the smoothed segmented volume and inputted it into the marching cube algorithm [94], which extracted an isosurface tessellated with ~300000 triangles. The number of triangles was then reduced to 200000 using the decimation algorithm [95]. Finally, the triangulated surface was deformed such that it lay in the middle of the gray matter by relaxing it against the smoothed segmented volume. We used the deformable template algorithm [92] for deformation. Finally, the resultant surface was visually inspected for positional accuracy and topological errors by overlapping it on the structural MR volume?. Extensive smoothing of the surface, which highlighted defects as sharp edges, was also performed to detect topological defects. If the surface was inaccurate or had defects, corrections were made in mrGray and subsequent processing was repeated. Reconstructed cortical surfaces were used to map or sample functional data. In addition, inflated, that is, hyper-smoothed versions of the reconstructed surface (Figure 2), were created for analysis of retinotopic organization. We used an inflation algorithm that was quite similar to that proposed by Fischl et al. (1999a)[96].

Appendix D. Generation of Probability Maps

Construction of volumetric models of retinotopic areas. The localized retinotopic areas were separated from one another and from other portions of the cortical surface. The isolated surfaces had no thickness, whereas the real cerebral cortex is about 2.5 mm thick on average, but exhibits regional variation (standard deviation) of 0.7 mm [97]. Here, we simplified cortical thickness to a constant 3 mm and incorporated this into the models of retinotopic areas by converting the surface models into volumetric ones with 3-mm thickness. The first step of this conversion was to compute the distance from the surface of each area to the points of an output volume. In the second step, the distance data were thresholded at half the distance of the assumed thickness to produce a draft version of the volumetric model for each area. In the final step, the draft models of different areas in one hemisphere were brought into a common space to detect where dilation caused overlap among them, and the overlapping voxels detected were removed from the models, producing a final volumetric model for each area. The volumetric model is a 3D binary array of voxels with each voxel having a label indicating the presence or absence of the area. We confirmed by visual inspection of 3D volume and surface-rendered models that each model did not overlap with the other models and lacked topological defects such as discontinuities and holes.

Talairach transformation. The volumetric models of retinotopic areas in each hemisphere were transformed into Talairach space using a single homogeneous transformation consisting of nine parameters, three translations, three rotations, and three scalings with respect to the axes of a cartesian frame. The Talairach coordinate system [98] has its origin at the superior edge of the anterior commissure (AC). In this system, a brain is scaled along X, Y, and Z axes. The X-axis (right to left) is defined by a line that runs through the origin and is orthogonal to the midline plane defined by the interhemispheric fissure. The Y-axis (anterior to posterior) is defined by a line that passes through the origin and the inferior edge of the posterior commissure (PC). The Z-axis (superior to inferior) is defined as a line that is orthogonal to the X- and Y-axes. We computed the homogeneous transformation matrix that converted each point in the volumetric models into a point in the Talairach system using a standard method [99]. First, the translation and rotation components of the matrix were computed from the locations of anatomical landmarks (AC, PC, and mid-sagittal plane) identified via visual inspection of the standard structural volume. The alignment was checked and corrected by graphically comparing the X, Y, and Z axes with three orthogonal slices of the standard volume and the reconstructed surface. Next, the scale components were determined by measuring the size of the brain along each of the three axes as the bounding box dimensions of the surface and then computing scaling factors to match the size to that of the 1988 Talairach atlas brain (X dimension: 136 mm; Y: 172 mm; Z: 118 mm). The scaling factor was determined separately for the left and right hemispheres. Since the Talairach atlas contains only a right hemisphere, the volumetric models for the left hemispheres were mirrored around the Y-axis and treated as though they were in right hemispheres.

Generation of the probability map. The probability of occurrence of each area in Talairach space was computed by counting the number of overlaps of the area's volumetric models in different hemispheres and dividing this by the total number of hemispheres (N = 10). This computation was repeated every 1 mm in Talairach space covering the visual cortex, and thus yielded a 3D probability map for each retinotopic area. Furthermore, the probability

maps for all the retinotopic areas were integrated into a maximum probability map, in which each voxel was assigned a label indicating which area had the greatest probability of being present there and was given the maximum value.

We visualized the 3D probability data in two ways, by mapping the data on orthogonal slices (Figure 4A) and on the surface (Figure 4B) of the Talairach brain. The slice representation was created for the same coronal, horizontal, and sagittal sections in the occipital region as those contained in the Talairach atlas. The surface representation was created by sampling the data at each node of the surface mesh, using a nearest neighbor algorithm within a radius of 2 mm. In both representations, probabilistic information was color-coded by assigning different colors to different areas, and by altering the brightness of colors such that increasing brightness corresponded to increasing probability.

The surface of the Talairach brain was reconstructed from a series of color tracings contained in the 1988 Talairach atlas in the form of coronal, horizontal, and sagittal sections. Each section was digitized using a flatbed scanner with a resolution of 150 dpi and segmented into three cortical structures, white matter, gray matter, and CSF, with decreasing integer labels in that order, using Photoshop software (Adobe Inc. San Jose, CA). The labels were the same as those used for the subjects' brains, as described above. All the segmented images for the orthogonal sections were resampled to volume data with 1 mm^3-resolution. We regarded this volume as the segmented volume of the Talairach brain, and reconstructed the Talairach surface in the same fashion as the subjects' brains, as described above.

Appendix E. Isoeccentricity Analysis

The fMRI signal was first sampled independently from each visual area delineated on the cortical surface reconstructed as a triangular mesh. For each node within a visual area, fMRI voxels were sampled from the cortical gray matter, except for the voxels located near the area boundary, and converted from raw intensity units to contrast, followed by omission of outliers.

The fMRI contrast responses from the phase encoding experiment for retinal eccentricities were analyzed spatially within each visual area, as a function of cortical geodesic distance along which retinotopic representation of visual field eccentricity shifted from the fovea to the periphery. First, for each node within the cortical mesh of a visual area, the shortest geodesic distance from the peripheral 16° contour was computed using Dijkstra's algorithm (Figure 5) [1, 100]. Second, using the distance information, the cortical mesh was divided into "iso-eccentricity bands" (3 mm width, 50% overlap) from posterior to anterior cortex, so that the eccentricity representation changed from fovea to periphery. Third, the fMRI responses were averaged within each iso-eccentricity band. Finally, the responses for different eccentricities were further averaged across repeated scanning sessions and stimulus cycles.

References

[1] Wandell BA, Chial S, Backus BT. Visualization and measurement of the cortical surface. J. *Cogn. Neurosci.* 2000 Sep;12(5):739-52.

[2] Van Essen DC, Dierker DL. Surface-Based and Probabilistic Atlases of Primate Cerebral Cortex. *Neuron.* 2007;56(2):209-25.
[3] Van Essen DC, Drury HA. Structural and functional analyses of human cerebral cortex using a surface-based atlas. *J. Neurosci.* 1997;17(18):7079.
[4] Lueck CJ, Zeki S, Friston KJ, Deiber MP, Cope P, Cunningham VJ, et al. The colour centre in the cerebral cortex of man. *Nature*. 1989;340(6232):386-9.
[5] Gulyás B. Functional organization of human visual cortical areas. In: Peters A, Jones EG, editors. *Cerebral Cortex Plenum Press*; 1997. p. 743-75.
[6] Courtney SM, Ungerleider LG. What fMRI has taught us about human vision. *Current Opinion in Neurobiology*. 1997;7(4):554-61.
[7] Grill-Spector K, Malach R. THE HUMAN VISUAL CORTEX. *Annual Review of Neuroscience*. 2004;27(1):649-77.
[8] Hubel DH, Wiesel TN. Uniformity of monkey striate cortex: a parallel relationship between field size, scatter, and magnification factor. *J. Comp. Neurol.* 1974 Dec 1;158(3):295-305.
[9] Dow BM, Snyder AZ, Vautin RG, Bauer R. Magnification factor and receptive field size in foveal striate cortex of the monkey. *Exp. Brain Res.* 1981;44(2):213-28.
[10] Wandell BA, Dumoulin SO, Brewer AA. Visual field maps in human cortex. *Neuron.* 2007 Oct 25;56(2):366-83.
[11] Sereno MI, Tootell RBH. From monkeys to humans: what do we now know about brain homologies? *Current Opinion in Neurobiology*. 2005;15(2):135-44.
[12] Yamamoto H, Fukunaga M, Takahashi S, Tanaka C, Ebisu T, Umeda M, et al., editors. BrainFactory: an integrated software system for surface-based analysis of fMRI data. *Human Brain Mapping 2002*; Sendai, Japan.
[13] Yamamoto H, Azukawa T, Takahashi S, Ejima Y. Software for surface-based analysis of fMRI. *IEICE Technical Report*, MBE2000-64. 2000;100(330):79-86.
[14] Yamamoto H, Fukunaga M, Tanaka C, Ebisu T, Umeda M, Ejima Y. Inconsistency and Uncertainty in the Locations of Human Visual Areas in Talairach Space: *Probability and Entropy Maps.* (in preparation).
[15] Yamamoto H, Ohtani Y. *Functional Brain Imaging and Visual Psychophysics*. Kougaku. 2004;33(2):80-8.
[16] Ejima Y, Takahashi S. Positioning of retinotopic areas and patterning of cerebral cortex layout. *Neuroreport*. 2005 Jan 19;16(1):9-12.
[17] Ejima Y, Takahashi S, Yamamoto H, Fukunaga M, Tanaka C, Ebisu T, et al. Interindividual and interspecies variations of the extrastriate visual cortex. *Neuroreport.* 2003 Aug 26;14(12):1579-83.
[18] Yamamoto H, Fukunaga M, Takahashi S, Azukawa T, Tanaka C, Ebisu T, et al. Anatomical and retinotopic organization of functional areas in the human visual cortex. *IEICE Technical Report*, MBE2000-65. 2000;100(330):87-94.
[19] Engel SA, Rumelhart DE, Wandell BA, Lee AT, Glover GH, Chichilnisky EJ, et al. fMRI of human visual cortex. *Nature*. 1994 Jun 16;369(6481):525.
[20] Sereno MI, McDonald CT, Allman JM. Analysis of retinotopic maps in extrastriate cortex. *Cereb. Cortex.* 1994 Nov-Dec;4(6):601-20.
[21] Tootell RB, Mendola JD, Hadjikhani NK, Ledden PJ, Liu AK, Reppas JB, et al. Functional analysis of V3A and related areas in human visual cortex. *J. Neurosci*. 1997 Sep 15;17(18):7060-78.

[22] Wandell BA, Brewer AA, Dougherty RF. Visual field map clusters in human cortex. *Philos. Trans R. Soc. Lond B Biol. Sci.* 2005 Apr 29;360(1456):693-707.
[23] Smith AT, Greenlee MW, Singh KD, Kraemer FM, Hennig J. The processing of first- and second-order motion in human visual cortex assessed by functional magnetic resonance imaging (fMRI). *J. Neurosci.* 1998 May 15;18(10):3816-30.
[24] Huk AC, Dougherty RF, Heeger DJ. Retinotopy and functional subdivision of human areas MT and MST. *J. Neurosci.* 2002 Aug 15;22(16):7195-205.
[25] Malach R, Reppas JB, Benson RR, Kwong KK, Jiang H, Kennedy WA, et al. Object-related activity revealed by functional magnetic resonance imaging in human occipital cortex. *Proc. Natl. Acad. Sci. USA.* 1995 Aug 29;92(18):8135-9.
[26] Larsson J, Heeger DJ. Two retinotopic visual areas in human lateral occipital cortex. *J. Neurosci.* 2006 Dec 20;26(51):13128-42.
[27] Levy I, Hasson U, Avidan G, Hendler T, Malach R. Center-periphery organization of human object areas. *Nat. Neurosci.* 2001 May;4(5):533-9.
[28] Zeki S. Improbable areas in the visual brain. *Trends in Neurosciences*. 2003;26(1):23-6.
[29] Hansen KA, Kay KN, Gallant JL. Topographic Organization in and near Human Visual Area V4. *J. Neurosci.* 2007 October 31, 2007;27(44):11896-911.
[30] Hadjikhani N, Liu AK, Dale AM, Cavanagh P, Tootell RB. Retinotopy and color sensitivity in human visual cortical area V8. *Nat. Neurosci.* 1998 Jul;1(3):235-41.
[31] Brewer AA, Liu J, Wade AR, Wandell BA. Visual field maps and stimulus selectivity in human ventral occipital cortex. *Nat. Neurosci.* 2005 Aug;8(8):1102-9.
[32] Wade AR, Brewer AA, Rieger JW, Wandell BA. Functional measurements of human ventral occipital cortex: retinotopy and colour. *Philos. Trans R. Soc. Lond B. Biol. Sci.* 2002 Aug 29;357(1424):963-73.
[33] Zeki S, Watson JD, Lueck CJ, Friston KJ, Kennard C, Frackowiak RS. A direct demonstration of functional specialization in human visual cortex. *J. Neurosci.* 1991 Mar;11(3):641-9.
[34] Bartels A, Zeki S. The architecture of the colour centre in the human visual brain: new results and a review. *Eur. J. Neurosci.* 2000 Jan;12(1):172-93.
[35] Pitzalis S, Galletti C, Huang RS, Patria F, Committeri G, Galati G, et al. Wide-field retinotopy defines human cortical visual area v6. *J. Neurosci.* 2006 Jul 26;26(30):7962-73.
[36] Sereno MI, Pitzalis S, Martinez A. Mapping of contralateral space in retinotopic coordinates by a parietal cortical area in humans. *Science.* 2001 Nov 9;294(5545):1350-4.
[37] Swisher JD, Halko MA, Merabet LB, McMains SA, Somers DC. Visual topography of human intraparietal sulcus. *J. Neurosci.* 2007 May 16;27(20):5326-37.
[38] Hasnain MK, Fox PT, Woldorff MG. Intersubject variability of functional areas in the human visual cortex. *Hum. Brain Mapp.* 1998;6(4):301-15.
[39] Amunts K, Malikovic A, Mohlberg H, Schormann T, Zilles K. Brodmann's areas 17 and 18 brought into stereotaxic space-where and how variable? *Neuroimage.* 2000 Jan;11(1):66-84.
[40] Dougherty RF, Koch VM, Brewer AA, Fischer B, Modersitzki J, Wandell BA. Visual field representations and locations of visual areas V1/2/3 in human visual cortex. *J. Vis.* 2003;3(10):586-98.

[41] Yamamoto H, Fukunaga M, Tanaka C, Umeda M, Ejima Y, editors. Inconsistency and Uncertainty in the Locations of Human Visual Areas in Talairach Space. *The 30th Annual Meeting of the Japan Neuroscience Society*; 2007; Yokohama, Japan. Elsevier.

[42] Yamamoto H, Fukunaga M, Tanaka C, Ebisu T, Umeda M, Ejima Y, editors. *A New Method for Quantifying Brain Structure-Function Relationships Based on Simultaneous Probability Map and Information Theory.* Society for Neuroscience 33rd Annual Meeting; 2003; New Orleans.

[43] Fukunaga M, Yamamoto H, Takahashi S, Tanaka C, Ebisu T, Umeda M, et al., editors. Functional and anatomical probabilistic maps of the human visual cortex [abstract]. *Human Brain Mapping*; 2002; Sendai.

[44] Wassle H, Grunert U, Rohrenbeck J, Boycott BB. Cortical magnification factor and the ganglion cell density of the primate retina. *Nature.* 1989;341(6243):643-6.

[45] Van Essen DC, Newsome WT, Maunsell JH. The visual field representation in striate cortex of the macaque monkey: asymmetries, anisotropies, and individual variability. *Vision Res.* 1984;24(5):429-48.

[46] Tootell RB, Switkes E, Silverman MS, Hamilton SL. Functional anatomy of macaque striate cortex. II. Retinotopic organization. *J. Neurosci.* 1988 May;8(5):1531-68.

[47] Daniel PM, Whitteridge D. The representation of the visual field on the cerebral cortex in monkeys. *J. Physiol.* 1961 Dec;159:203-21.

[48] Rosa MGP. Visuotopic organization of primate extrastriate cortex. In: Rockland KS, Kaas JH, Peters A, editors. *Cerebral Cortex*. New York, NY: Plenum; 1997.

[49] Maeda K, Fukunaga M, Nakagoshi A, Yamamoto H, Matsuno T, Tanaka C, et al. Isoeccentricity averaging: a new analytical technique for fMRI studies on human visual processing [ABSTRACT]. *Neuroscience Research.* 2003;46(Supplement 1):S57.

[50] Boynton GM, Engel SA, Glover GH, Heeger DJ. Linear systems analysis of functional magnetic resonance imaging in human V1. J. *Neurosci.* 1996 Jul 1;16(13):4207-21.

[51] Schwartz EL. Computational anatomy and functional architecture of striate cortex: a spatial mapping approach to perceptual coding. *Vision Res.* 1980;20(8):645-69.

[52] Schwartz EL. Topographic Mapping in Primate Visual Cortex: History, Anatomy, and Computation. In: Kelly DH, editor. *Visual science and engineering: models and applications*. New York: M. Dekker; 1994. p. 293-359.

[53] Sereno MI, Dale AM, Reppas JB, Kwong KK, Belliveau JW, Brady TJ, et al. Borders of multiple visual areas in humans revealed by functional magnetic resonance imaging. *Science*. 1995 May 12;268(5212):889-93.

[54] Schira MM, Wade AR, Tyler CW. Two-dimensional mapping of the central and parafoveal visual field to human visual cortex. *J. Neurophysiol.* 2007 Jun;97(6):4284-95.

[55] Slotnick SD, Klein SA, Carney T, Sutter EE. Electrophysiological estimate of human cortical magnification. *Clin. Neurophysiol.* 2001 Jul;112(7):1349-56.

[56] Yoshor D, Bosking WH, Ghose GM, Maunsell JHR. Receptive Fields in Human Visual Cortex Mapped with Surface Electrodes. *Cereb Cortex.* 2007 October 1, 2007;17(10):2293-302.

[57] Horton JC, Hoyt WF. The representation of the visual field in human striate cortex. A revision of the classic Holmes map. *Arch. Ophthalmol.* 1991 Jun;109(6):816-24.

[58] Beard BL, Levi DM, Klein SA. Vernier acuity with non-simultaneous targets: the cortical magnification factor estimated by psychophysics. *Vision Res.* 1997 Feb;37(3):325-46.

[59] Rovamo J, Virsu V. Isotropy of cortical magnification and topography of striate cortex. *Vision Res.* 1984;24(3):283-6.

[60] Kastner S, De Weerd P, Pinsk MA, Elizondo MI, Desimone R, Ungerleider LG. Modulation of sensory suppression: implications for receptive field sizes in the human visual cortex. *J. Neurophysiol.* 2001 Sep;86(3):1398-411.

[61] Smith AT, Singh KD, Williams AL, Greenlee MW. Estimating Receptive Field Size from fMRI Data in Human Striate and Extrastriate Visual Cortex. *Cereb Cortex.* 2001 December 1, 2001;11(12):1182-90.

[62] McLlwain JT. Point images in the visual system: new interest in an old idea. *Trends in Neurosciences.* 1986;9:354-8.

[63] Heeger DJ, Ress D. What does fMRI tell us about neuronal activity? *Nat. Rev. Neurosci.* 2002;3(2):142-51.

[64] Grinvald A, Lieke EE, Frostig RD, Hildesheim R. Cortical point-spread function and long-range lateral interactions revealed by real-time optical imaging of macaque monkey primary visual cortex. *J. Neurosci.* 1994 May;14(5 Pt 1):2545-68.

[65] Bonhoeffer T, Grinvald A. Optical imaging based on intrinsic signals: the methodology. In: Toga AW, Mazziotta JC, editors. *Brain Mapping: the Methods.* San Diego Academic Press; 1996. p. 55–97.

[66] Gilbert CD, Das A, Ito M, Kapadia M, Westheimer G. Spatial integration and cortical dynamics. *Proceedings of the National Academy of Sciences.* 1996 January 23, 1996;93(2):615-22.

[67] Tanigawa H, Wang Q, Fujita I. Organization of Horizontal Axons in the Inferior Temporal Cortex and Primary Visual Cortex of the Macaque Monkey. *Cereb Cortex.* 2005 December 1, 2005;15(12):1887-99.

[68] Cannon MW, Fullenkamp SC. Spatial interactions in apparent contrast: inhibitory effects among grating patterns of different spatial frequencies, spatial positions and orientations. *Vision Res.* 1991;31(11):1985-98.

[69] Ejima Y, Takahashi S. Apparent contrast of a sinusoidal grating in the simultaneous presence of peripheral gratings. *Vision Res.* 1985;25(9):1223-32.

[70] Goda N, Fukunaga M, Yamamoto H, Tanaka C, Ebisu T, Umeda M, et al., editors. Orientation-dependent lateral interactions in human visual areas: an fMRI study. *The 24th Annual Meeting of the Japan Neuroscience Society*; 2001; Kyoto, Japan. Elsevier.

[71] Ejima Y, Takahashi S, Yamamoto H, Goda N. Visual Perception of Contextual Effect and Its Neural Correlates In: Funahashi S, editor. *Representation and Brain.* Tokyo: Springer Verlag; 2007. p. 3-20.

[72] Williams AL, Singh KD, Smith AT. Surround Modulation Measured With Functional MRI in the Human Visual Cortex. *J. Neurophysiol.* 2003 January 1, 2003;89(1):525-33.

[73] Ohtani Y, Okamura S, Yoshida Y, Toyama K, Ejima Y. Surround suppression in the human visual cortex: an analysis using magnetoencephalography. *Vision Res.* 2002 Jul;42(15):1825-35.

[74] Zenger-Landolt B, Heeger DJ. Response suppression in v1 agrees with psychophysics of surround masking. *J. Neurosci.* 2003 Jul 30;23(17):6884-93.

[75] Lamme VA, Roelfsema PR. The distinct modes of vision offered by feedforward and recurrent processing. *Trends Neurosci.* 2000 Nov;23(11):571-9.

[76] Super H, Spekreijse H, Lamme VA. Two distinct modes of sensory processing observed in monkey primary visual cortex (V1). *Nat. Neurosci.* 2001 Mar;4(3):304-10.

[77] Ban H, Fukunaga M, Nakagoshi A, Yamamoto H, Tanaka C, Ebisu T, et al. Relations between retinotopic organization of human low-level visual regions and position-invariance object perception – an fMRI study –. *IEICE Technical Report*, HIP2003-127. 2004 Aug 23;103(743):5-10.

[78] Ban H, Yamamoto H, Fukunaga M, Nakagoshi A, Tanaka C, Ebisu T, et al. Global shape processing in human early visual cortex. *VISION.* 2005 Aug 23;17(3):191-4.

[79] Ban H, Yamamoto H, Fukunaga M, Nakagoshi A, Umeda M, Tanaka C, et al. Toward a common circle: interhemispheric contextual modulation in human early visual areas. *J. Neurosci.* 2006 Aug 23;26(34):8804-9.

[80] Ban H, Yamamoto H, Saiki J, editors. Retinotopy-based morphing of brain activity. *The 29th Annual Meeting of the Japan Neuroscience Society*; 2006; Kyoto, Japan. Elsevier.

[81] Goldstein EB. Cross-Talk Between Psychophysics and Physiology in the Study of Perception In: Goldstein EB, editor. *Blackwell handbook of perception.* Oxford, UK ; Malden, Mass.: Blackwell; 2001. p. 1-23.

[82] Teller DY. Linking propositions. *Vision Res.* 1984;24(10):1233-46.

[83] Schiller PH. *Past and Present Ideas About How the Visual Scene is Analyzed by the Brain.* In: Peters A, Jones EG, editors. Cerebral Cortex Plenum Press; 1997. p. 59-90.

[84] Hasson U, Harel M, Levy I, Malach R. Large-scale mirror-symmetry organization of human occipito-temporal object areas. *Neuron.* 2003;37(6):1027.

[85] Hasson U, Levy I, Behrmann M, Hendler T, Malach R. Eccentricity bias as an organizing principle for human high-order object areas. *Neuron.* 2002;34(3):479.

[86] Yamamoto H. *The development of a software system for computational neuroimaging and its applications to visual sicience* [Doctoral thesis]. Kyoto, Japan: Kyoto University; 2001.

[87] Ban H. *Neural processing of Spatiotemporal Visual Contexts in Human Retinotopic Early Visual Areas: fMRI studies* [Doctoral thesis]. Kyoto, Japan: Kyoto University; 2007.

[88] DeYoe EA, Bandettini P, Neitz J, Miller D, Winans P. Functional magnetic resonance imaging (FMRI) of the human brain. *J. Neurosci. Methods.* 1994 Oct;54(2):171-87.

[89] Engel SA, Glover GH, Wandell BA. Retinotopic organization in human visual cortex and the spatial precision of functional MRI. *Cereb Cortex.* 1997 Mar;7(2):181-92.

[90] Brockwell PJ, Davis RA. *Time series: theory and methods.* 2nd ed. New York: Springer-Verlag; 1991.

[91] Drury HA, Van Essen DC, Corbetta M, Snyder AZ. *Surface-based analyses of the human cerebral cortex.* In: Toga AW, editor. Brain Warping San Diego: Academic Press; 1999. p. 337-63.

[92] Dale AM, Sereno MI. Improved localization of cortical activity by combining EEG and MEG with MRI cortical surface reconstruction: A linear approach. *J. Cogn. Neurosci.* 1993;5(2):162-76.

[93] Teo PC, Sapiro G, Wandell BA. Creating connected representations of cortical gray matter for functional MRI visualization. *IEEE Transactions on Medical Imaging.* 1997;16(6):852-63.

[94] Lorensen W, E. , Cline H, E. . Marching cubes: A high resolution 3D surface construction algorithm. *Proceedings of the 14th annual conference on Computer graphics and interactive techniques*; 1987. ACM Press; 1987.

[95] Schroeder W, J. , Zarge J, A., Lorensen W, E. . Decimation of triangle meshes. *Proceedings of the 19th annual conference on Computer graphics and interactive techniques*; 1992. ACM Press; 1992.

[96] Fischl B, Sereno MI, Dale AM. Cortical surface-based analysis. II: Inflation, flattening, and a surface-based coordinate system. *Neuroimage.* 1999 Feb;9(2):195-207.

[97] Fischl B, Dale AM. Measuring the thickness of the human cerebral cortex from magnetic resonance images. *Proc. Natl. Acad. Sci. USA*. 2000 Sep 26;97(20):11050-5.

[98] Talairach J, Tournoux P. *Co-Planar Stereotactic Atlas of the Human Brain*. Stuttgart/New York: Thieme; 1988.

[99] Desmond JE, Lim KO. On- and offline Talairach registration for structural and functional MRI studies. *Human Brain Mapping*. 1997;5(1):58-73.

[100] Dijkstra EW. A note on two problems in connexion with graphs. *Numerische Mathematik.* 1959;1(1): 269 - 71.